Journal of Applied and Natural Science
18(1), 37 - 50 (2026)
ISSN : 0974-9411 (Print), 2231-5209 (Online)
journals.ansfoundation.org

Research Article

Synthesis, chemical characterization and antimicrobial efficacy of chemically synthesized iron oxide nanoparticles (IONPs) against multidrug-resistant bacteria

Raman Nadar Laura*
Department of Microbiology, Malankara Catholic College, Mariagiri, affiliated to Manonmaniam Sundaranar University, Abishekapatti, Tirunelveli -627012, Tamil Nadu, India
K. R. Beula Rani
Department of Microbiology, Malankara Catholic College, Mariagiri, affiliated to Manonmaniam Sundaranar University, Abishekapatti, Tirunelveli -627012, Tamil Nadu, India

*Corresponding author. E-mail: lauraramannadar@gmail.com

Article Info
https://doi.org/10.31018/jans.v18i1.7084
Received: August 09, 2025
Revised: January 27, 2026
Accepted: February 04, 2026

How to Cite
Laura, R.N. and Rani, K.R.B. (2026). Synthesis, chemical characterization and antimicrobial efficacy of chemically synthesized iron oxide nanoparticles (IONPs) against multidrug-resistant bacteria. *Journal of Applied and Natural Science*, 18(1), 37 - 50. https://doi.org/10.31018/jans.v18i1.7084

Abstract
The discipline of nanobiotechnology has become the most studied field in helping the medical field to develop drugs against multidrug-resistant bacteria. Chemically synthesized iron oxide nanoparticles (IONPs) are produced by various methods alternatives of typical antibiotics. In the present research IONPs were chemically synthesized, characterized and applied against medically important bacteria. Transmission Electron Microscopy (TEM) and Scanning Electron Microscopy (SEM) were used to observe the nanoparticles' morphology, which showed a spherical or quasi-spherical shape with a size range of ± 10 nm. Ultraviolet-visible spectroscopy (UV-Vis) and Fourier Transform Infrared Spectroscopy (FTIR) were used to analyse the functional groups and the elements present in the sample, and Nuclear Magnetic Resonance (NMR), X-Ray Diffraction (XRD) and X-Ray Photoelectron Spectroscopy (XPS) were used to analyse the crystalline structure. Antibacterial activity of the nanoparticles against four pathogenic strains: *Pseudomonas aeruginosa (P. aeruginosa-424), Staphylococcus aureus (S. aureus-902*), *Streptococcus mutans (S. mutans-497*), and *Escherichia coli* (*E. coli-443*) was investigated by microbiological assays. Concentration-dependent inhibition zones, low minimum inhibitory concentrations (MICs), and notable biofilm damage were among the main methods. Time-kill assays and DNA fragmentation investigations indicated that the chemically synthesised iron oxide nanoparticles have the potential to induce bacterial cell death. Among the species investigated, S. aureus was more sensitive to IONPs, which caused DNA damage. The study highlights how IONPs are a promising candidate for inclusion in antibacterial medications.

Keywords: Iron oxide nanoparticles, Microbiological assays, Multidrug-resistant bacteria, Structural characterization

INTRODUCTION

Nanoparticles, especially iron oxide nanoparticles (IONPs), also called “superparamagnetic iron oxide nanoparticles,” have several properties that make them useful in the biological environment. Most of their sizes range from 1 to 100 nm, making them selective for many medical applications, such as tumour penetration, biodistribution, and therapeutic efficacy (Gupta *et al*., 2024; Bashiru *et al*., 2023). Nanoparticles are entering the research field, merging with medical, pharmaceutical, biological, technological, environmental, agricultural, cosmetic, and many other fields. Their potentiality may vary depending on the external environment. Their properties vary depending on the mode of synthesis, which can be chemical or green (Maria *et al*., 2023). Since these conditions can affect IONP’s efficacy, stability, mobility, chemical and physical characteristics, the synthesis process is crucial. Chemical, physical, and biological synthesis procedures are examples of these synthetic techniques. IONPs with superior crystallinity, defined structure, and controlled morphology are focused while choosing different methods. To achieve the ideal morphological characteristics, the optimisations are carried out by adjusting several factors, including surfactant and solvent types, reaction time, ageing period, and temperature. This approach is thought to be among the most effective ways to allow IONPs with similar properties to evolve (Priyanka *et al.,* 2024). Because IONPs exhibit superparamagnetic be-

haviour, their sensitivity to external magnetic fields enables their use in targeted delivery, improving drug or gene delivery precision and ensuring higher therapeutic concentrations at the desired site (Sathyadevi and Yun-Ming, 2019). Antibiotic resistance has become one of the biggest hurdles in the medical scenario. Therefore, novel methods of overcoming this issue are essential today.The present study aimed to synthesize and characterize iron oxide nanoparticles using advanced spectroscopic and microscopic techniques (SEM, TEM, UV-Vis, FTIR, XRD, XPS and NMR). Their antibacterial and antibiofilm activities against clinically relevant pathogenic bacteria are evaluated through several microbiological assays with the ultimate goal of understanding their mechanism of action and assessing their potential as alternative antimicrobial agents.

MATERIALS AND METHODS

Chemically synthesized IONPs were employed in this research against four bacterial strains namely *Staphylococcus aureus*, *Pseudomonas aeruginosa*, *Streptococcus mutans* and *Escherichia coli*.

Chemical synthesis of iron oxide nanoparticles

In the present study, iron oxide nanoparticles (IONPs) were chemically synthesized using the modified procedure reported by Justin *et al*. (2017). Accordingly, Ferric chloride ($FeCl_3$) and Ferrous sulfate ($FeSO_4$) were used as the iron sources and Tetramethyl Ammonium Hydroxide ($C_4H_{13}NO$) as the reducing agent. 0.1g of $FeCl_3$ and $FeSO_4$ were dissolved in 1mL of double distilled water respectively. The solutions were vortexed for two minutes. The clear solutions were pipetted out and were mixed together. This iron source was poured drop by drop into Tetramethyl ammonium hydroxide in the ratios $500\mu L$:$100\mu L$; $500\mu L$:$200\mu L$; $500\mu L$:$300\mu L$; $500\mu L$:$400\mu L$; $500\mu L$:$500\mu L$, and vortexed for five minutes. The obtained black precipitate was kept undisturbed for 5 minutes. The resultant supernatant of $500\mu L$:$500\ \mu L$ batch was found with IONPs optically reflecting against the magnetic field, which was then pipetted out for further use. The particles were separated with the help of bar-magnet with a strength of 50 Gauss. The obtained particles were washed three times with double distilled water for microbial studies. The unused particles were preserved by dispersing them in Formaldehyde.

Microscopy analysis

Scanning electron microscope (SEM)

SEM analysis was performed using the Carl Zeiss EVO 18 Research instrument at the Central Laboratory for Instrumentation and Facilitation (CLIF, Kerala University). A drop of analytic IONPs was dried on a silicon wafer prior to observation (Rimbu, 2025).

Transmission electron microscope (TEM)

TEM analysis was performed using the JEOL JEM-200 instrument at the CSIR - National Institute for Interdisciplinary Science and Technology (NIIST, Thiruvananthapuram). The sample was loaded on a 3 mm carbon-coated copper grid and allowed to dry prior to observation (Heggen, 2025).

Spectroscopy analysis

UV-Visible-NIR spectroscopy

UV-Vis analysis was performed using a Thermo Scientific Nicolet iS50 spectrophotometer at the Central Laboratory for Instrumentation and Facilitation (CLIF, University of Kerala). The absorbance value was obtained from 200 nm to 800 nm (Alok, 2025).

Fourier transform infrared spectroscopy (FTIR)

FTIR analysis was performed using a Thermo Scientific iS50 FT-IR spectrometer at the Central Laboratory for Instrumentation and Facilitation (CLIF, University of Kerala). A drop of the analytical sample was placed on a glass slide, and a transition-mode scan was used to record the spectrum in the 4000-500 cm-1 region (Rimbu, 2025).

X-Ray diffraction (XRD)

XRD analysis was performed using a Bruker D8 ADVANCE with DAVINCI at the Central Laboratory for Instrumentation and Facilitation (CLIF, University of Kerala). A thin film of the sample was dried on a glass slide, and the spectrum was obtained (Aarti *et al.,* 2025).

X-Ray photoelectron spectroscopy (XPS)

XPS reading was done in Thermo Scientific™ ESCALAB™ Xi+, Central Laboratory for Instrumentation and Facilitation (CLIF-University of Kerala). Spectral values for metal (iron), oxygen, carbon and nitrogen were recorded. These elements were desired to be observed because, while employing chemical synthesis methods, it is surmised that intercalating elements may become embedded in IONPs (Gregory *et al.,* 2025).

Nuclear magnetic resonance (NMR)

NMR analysis was performed using a Bruker Avance 400 MHz FT-NMR spectrometer at the Central Laboratory for Instrumentation and Facilitation (CLIF, University of Kerala). The solvent used was D2O, and the spectrum was obtained for hydrogen (1H-NMR) (Adel *et al.*, 2025).

Microbiological analysis

Antibacterial activity: Agar- well diffusion method

The medium was prepared by dissolving 3.8 g of the

commercially available Mueller-Hinton agar in 100 mL of distilled water. The dissolved medium was autoclaved at 15 lbs pressure at 121°C for 15 minutes. The autoclaved medium was mixed well and poured onto 100mm petriplates (25-30ml/plate) while still molten. Petri plates containing 20 ml of Mueller-Hinton agar medium were seeded with a 24-hour culture of bacterial strains. Wells were cut, and the test sample iron oxide (500, 250, 100, and 50 µg/mL) was added. The plates were then incubated at 37°C for 24 hours. Antibacterial activity was assayed by measuring the diameter of the inhibition zone around each well. Gentamicin was used as a positive control. All the tests were done in triplicates (Bauer *et al.,* 1959).

Determination of minimum inhibitory concentration (MIC); Minimum bactericidal concentration (MBC)

The broth microdilution assay method was used to determine the MICs for the four bacterial strains (*S. mutans-497*, *S. aureus-902*, *E. Coli-443*, and P. aeruginosa-424, purchased from MTCC, Chandigarh, India) in sterile disposable flat-bottomed 96-well microtiter plates, and the susceptibility of the organisms was investigated. Briefly, the 0.5 McFarland inoculum suspensions were further diluted 1:100 in nutrient broth before inoculation. 50 µL of the bacterial suspension was then seeded into a 96-well plate containing 50 µL of the test sample at serial concentrations. The final concentrations of FeO were 1000, 500, 250, 125, 62.5, 31.25, 15.6, 7.8, 3.9 and 1.9 µg/mL. The plates were then incubated at 37 °C for 18–24 h. The results were read at 600 nm using a microplate reader. Changes of colour were observed and recorded. All the tests were done in triplicates. (Gang *et al.,* 2021). To determine the MBC, 10µL from the MIC-negative well (no visible turbidity) was spread into nutrient agar plates and incubated for 24 hours at 37 °C.

Time killer assay

The time-kill assay method was used to assess the bactericidal activity at varying concentration over time. Nutrient broth along with 10ml of the test organism suspension, was introduced into the 15mL tube and IC50 Concentration (50.16µg/mL for *S. aureus*, 59.57 µg/mL for *S. mutans*, 135.3 µg/mL for *E. coli* and 156.1 µg/mL for *P. aeruginosa*) of the test iron oxide was added. For negative control, 9 ml sterile distilled water and 1ml of the test organism was added. The plates were then incubated at 37 °C for 24 h. The results were observed every 1, 6, 12 and 24 hrs. Then the results were read at 600 nm using a Calorimeter. Colour changes were observed and recorded. The reduction in microbial population was calculated using GraphPad Prism 8 software. (Tsuji *et al.,* 2008)

Antibiofilm assay

To evaluate the efficacy of the drug in interrupting biofilm formation, the MTP assay was carried out as described by Christensen *et al*. (1985) using 96-well flat-bottom polystyrene titration plates. Individual wells were filled with 180 µL of BHI broth, followed by inoculation with 10 µL of an overnight pathogenic bacterial culture. To this 10 µL sample, iron oxide was added from the prepared stock solutions at 1000, 500, 250, 125, 62.5, 31.25, 15.6, 7.8, 3.9, and 1.9 µg/mL, along with a control (without test sample), and the mixture was incubated at 37°C for 24 h. After incubation, the contents of the wells were removed and washed with 0.2 mL of phosphate-buffered saline (PBS) pH 7.2 to remove free-floating bacteria. The adherence of sessile bacteria was fixed with sodium acetate (2%) and stained with crystal violet (0.1%, w/v). Excessive stain was removed by deionized water wash and kept for drying. Further, dried plates were washed with 95% ethanol and optical density was determined using a microtitre plate reader (Thermo) at 600 nm. The percentage of biofilm inhibition was calculated using the below formula (Wang *et al.,* 2010).

$$\% \text{ Biofilm inhibition} = \frac{\text{Control OD- Test OD}}{\text{Control OD}} \times 100$$

DNA fragmentation

The sample was tested, treated, using the two best organisms; *P. aeruginosa* and *S. aureus*. Briefly, the cultured *P. aeruginosa* and *S. aureus* (1ml) were treated with the IC50 concentration of the test sample incubator for 24 h. After the incubation period, total *P. aeruginosa* and *S. aureus* culture were collected in a centrifuge tube.

The samples were placed in 2mL tubes separately, and then 875 µL of TE Buffer and 10% of 100 µL SDS were added. Homogenized the sample with sterile homogenizer. And 5 µL of Proteinase K (20 mg/mL) was added. The mixture was incubated at a cool temperature for 30-60 minutes (with occasional mixing/quick vortex) to facilitate digestion. After complete digestion, 1mL of Phenol Chloroform was added and then the samples were centrifuged at 12000 rpm for 10 minutes. After that, about 500 µL of clear supernatant were collected into a new- labeled 2mL tube. Then 100µL of 5M Sodium acetate were added and the volume was made up to 2 ml with Isopropanol to precipitate the DNA. Then the samples were centrifuged at 12,000 rpm for 10 minutes. After that, the supernatant was removed and 1ml of ice-cold 70% ethanol was added to the pellets for washing. Sample was spun at 12000 rpm, for 5 minutes. Carefully removed the supernatant, then pipetted out excess liquid and allowed it to partially dry

with the lid off at room temperature. Partially dried DNA was resuspended in 20- 30 µL of 1x TE buffer (Sambrook *et al.,* 2001).

RESULTS AND DISCUSSION

Scanning electron microscope (SEM)

The SEM image (Fig. 1) is shown with a 200 nm scale bar. The image was slightly blurred and aggregated forming clusters rather than individually separated particles. The aggregation would be due to magnetic attraction between the particles and other forces, such as van der Waals forces. The aggregation could be around 20-100nm.

Transmission electron microscope (TEM)

TEM images (Fig. 2, (a) and (b)) are given in 20 nm and 10 nm scale bars respectively. Based on Fig. 2(a), the individual nanoparticles appeared to be roughly±10 nm in diameter. Most particles fall within this nanoscale range. The particles appear mostly spherical to quasi-spherical shapes. Some particles appeared with irregular edges indicating minor size variations. The image also appears to show loosely packed clusters rather than highly fused ones. The Fig. 2 (b) is given in a 10 nm scale which exhibits its quasi-spherical morphological structure.

UV-Visible spectroscopy (UV-Vis)

Covers both UV (200-400 nm) and visible (400-800 nm) regions. A peak is seen from 205nm. The curve shows a steep rise in absorbance below 400 nm (UV region), which is characteristic of: Iron oxide nanoparticles (Fe_3O_4/γ-Fe_2O_3 typically absorb at 300-400 nm). Possible organic capping agents (if absorbance peaks at 200-300 nm) (Fig. 3). Silvia *et al.* (2017) reported that "the aqueous solution of FeSO4 exhibits a continuous absorption band throughout the spectrum and lacks a peak". "A distinct absorption band observed at 329 nm confirmed the successful formation of IONPs, consistent with the characteristic surface plasmon resonance of iron oxide nanostructures" was observed and reported by Muhammad *et al. (*2024).

Fourier transform infrared spectroscopy (FTIR)

Analysis using Fourier Transform Infrared Spectroscopy (FTIR) reveals details about the material's molecular structure and chemical bonding. At ambient temperature, FTIR measurements are made in the 400–4000 cm-1 range to analyse the crystalline nature and composition of the chemically produced iron oxide nanoparticles.

The FTIR spectrum of SPIONs shows prominent absorption bands between 3263.38 and 1099.93 cm-1, which is considered the fingerprint region for iron oxide

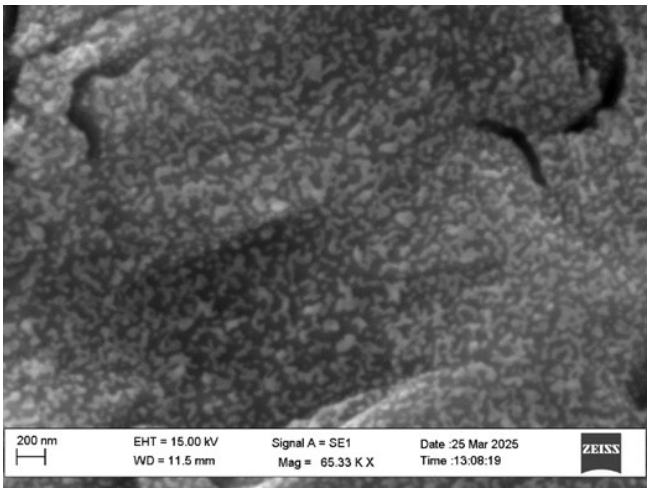

Fig. 1. *SEM image of IONPs*

nanoparticles. A broad Peak is seen at ~3263.38 cm^{-1} which shows O-H stretching from adsorbed water molecules or surface hydroxyl groups (Fig. 4). Darezereshki (2011) reported the stretching and bending vibrations of the hydroxyl groups and/or water molecules, responsible for the extremely broad absorption band centred at 3331 cm^1 and peaking at 1625 cm^1.

A peak at ~1636.74 cm^{-1} confirms the presence of water molecules. And a strong band at 500-700 cm^{-1} which determine the presence of inorganic compound (fingerprint region for iron oxides): ~490 cm^{-1}: Magnetite (Fe_3O_4). As per Kamath *et al.,* (2020) report, "the bonds that form between the iron and oxygen in the sample are shown by wavelengths between 450 and 950 cm1".

X-Ray diffraction (XRD)

To demonstrate the crystallinity of the chemically synthesized iron oxide nanoparticles, XRD method is performed. These 3 peaks (35.586°, 57.174°, and 62.847°) observed in this spectrum indicate crystallinity, as evidenced by their sharpness (Fig. 5). In their study, Rajeshkumar *et al.,* (2024) conducted X-ray diffraction (XRD) analysis on synthesized iron oxide nanoparticles and observed "distinct diffraction peaks at 2θ angles of 31.8°, 35.2°, and 35.4° and their systematic referencing to the crystallographic planes confirmed that a ferrite structure (either maghemite, γ-Fe□O□, or magnetite, Fe□O□) had formed". Similarly, Johar *et al.,* (2024) stated that the trigonal structure of magnetite was identified as the cause of peaks at 49.75° (300) and 56.74° (009) and additionally, these included peaks at 30.17° (220), 31.76 (202), 35.43° (311), 43.14° (400), 48.31° (331), 62.65° (440), and 66.31° (531), which corresponded to cubic magnetite.

X-Ray photoelectron spectroscopy (XRD)

To help interpret the XRD data and to investigate the surface structures of the IONPs, X-ray photoelectron

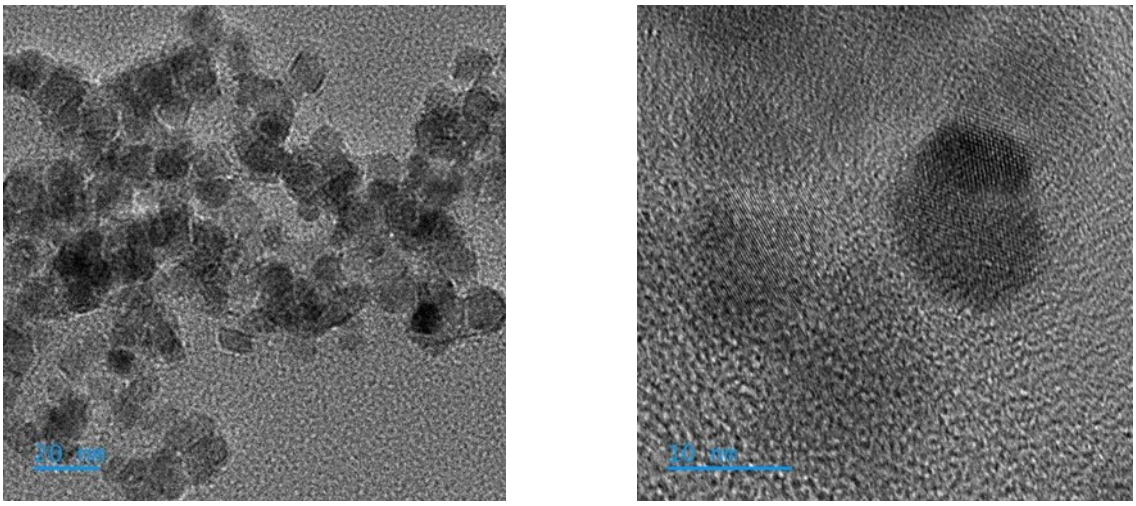

a b

Fig. 2. *(a) and (b),Transmission electron microscopy (TEM) images of chemically produced iron oxide nanoparticles (IONPs)*

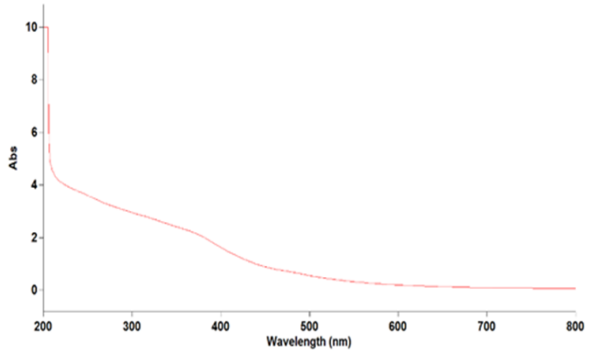

Fig. 3. *Ultraviolet-visible spectroscopy (UV-VIS) spectrum of iron oxide nanoparticles*

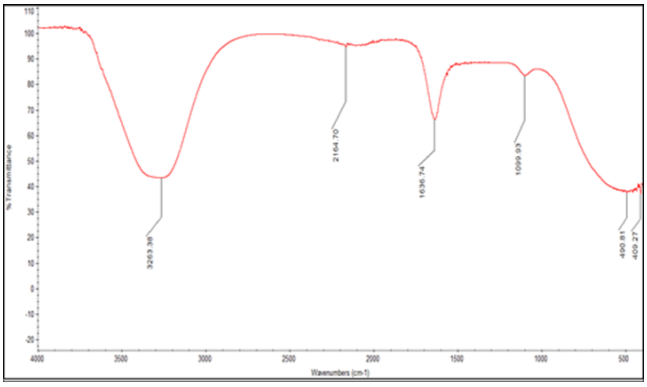

Fig. 4. *Fourier transform infrared spectroscopy (FTIR) spectrum of iron oxide nanoparticles*

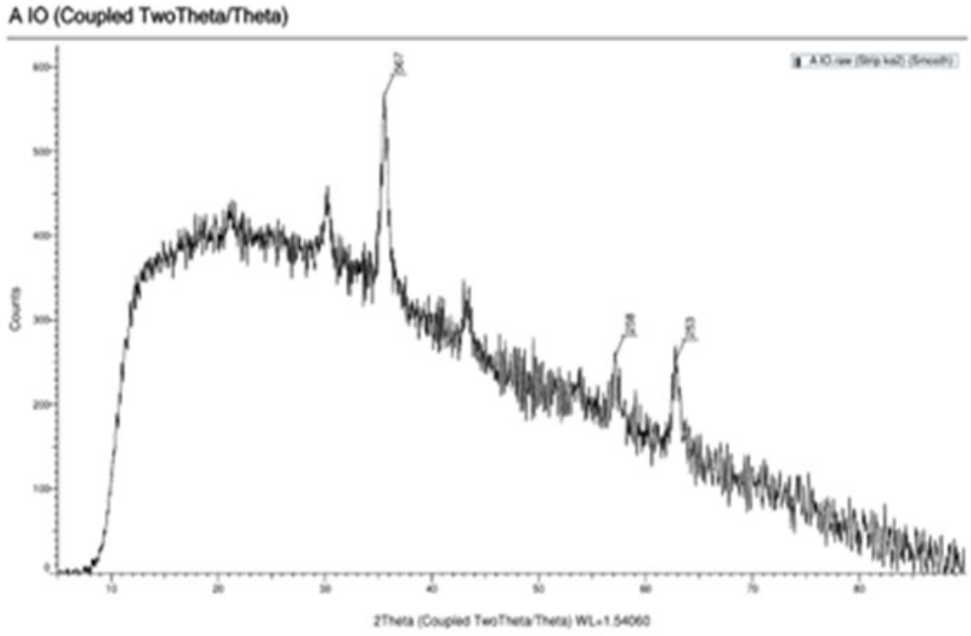

Fig. 5. *X-Ray diffraction (XRD) spectrum of chemically synthesized iron oxide nanoparticles*

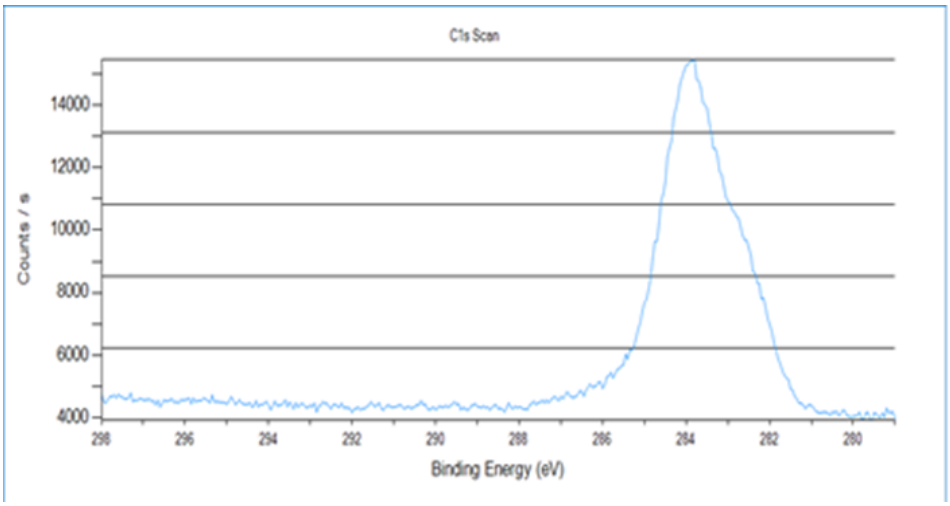

Fig. 6. *X-Ray Photoelectron Spectroscopy (XPS) of carbon element*

spectroscopy (XPS) was performed. The binding energy for carbon was observed. The peak ~284 eV is commonly attributed to carbon-carbon (C-C) bonds. (Fig. 6). In the Fe XPS spectrum, 2 peaks can be observed at ~707 eV and ~721 eV, which affirm the presence of metal oxide. The Fe2p spectrum strongly matches Fe3+ (Hematite like). The shape also suggests mixed multiplet structure of metal oxide. (Fig. 7). The peak observed at ~400 eV shows the presence of C-NH2(Fig. 8). A strong peak is observed in the oxygen XPS spectrum at ~527 eV, confirming the presence of a metal oxide (Fig. 9). Bristy *et al.,* (2024), reported that "the peak in the narrow scan for oxygen at the binding energy 529.7 eV was attributed for lattice Fe3+-O bonded oxygen. They also added that the distinctive peaks of the 3+ ion of γ-Fe_2O_3 are located at 710.31 and 724.48 eV and the lattice Fe3+-O bound oxygen was identified as the source of the peak in the oxygen narrow scan at the binding energy 529.7 eV".

Nuclear magnetic resonance (NMR)

Two peaks were observed at 5.569 and 4.679, suggesting the potential presence of water molecules or organic ligands. One analytical technique for determining a compound's structure based on the type of proton or hydrogen present is 1H-NMR spectroscopy (Fig. 10). The number of proton types in a chemical and the environmental characteristics of each kind of hydrogen proton are revealed by the 1H-NMR spectra, claimed by Laurence and Timothy (2017).

Antibacterial activity

Using the agar well diffusion method, the study tested the antibacterial effect of iron oxide (FeO) nanoparticles against four bacterial strains: *S. aureus-902*, *S. mutans -497*, *E. coli-443*, and *P. aeruginosa-424,* purchased from MTCC, Chandigarh, India. Gentamicin, the positive control, produced a bigger zone of inhibition (16.1–17.35 mm). Maximum activity is recorded at 1000 µg/mL (Fig. 11, 12, 13 and 14)(Table 1). Notably, *S. aureus* and *P. aeruginosa* did not show any inhibition below 500 µg/mL (Figs.11 and 14) , although *S. mutans* and *E. coli* maintained partial activity at 250 µg/mL (ZOI: 7.6 ± 0.14 mm and 8.1 ± 0.14 mm, respectively) (Figs.12 and 13). Hend *et al.,* (2024) mentioned that "iron oxide nanoparticles enter bacterial cells and produce ROS, which stops biofilm development". Sahar *et al.,* (2025) conducted an antibacterial method where "Gram-positive, *Staphylococcus aureus* (15.2 ± 0.8 mm at 64 µg/mL) was more sensitive than Gram-negative strains, most likely because the nanoparticles adhered better to their thicker peptidoglycan coatings. Among Gram-negative bacteria, *Escherichia coli* was the least responsive (12.11 ± 0.3 mm), whereas *Pseudomonas aeruginosa* shown exceptional susceptibility (16.23 ± 0.5 mm at 64 µg/mL)". On the other hand, in the findings of Abdulrahman *et al.,* (2024), "gram-negative bacteria demonstrated significant susceptibility, with *E. coli* showing maximum inhibition zones of 15 mm at 100 mg/mL whereas *P. aeruginosa* exhibited even greater sensitivity, producing 26 mm inhibition zones at 100 mg/mL while maintaining activity at 6.25 mg/mL, though no inhibition was observed at 3.125 mg/mL".

Minimum inhibition concentration (MIC) and minimum bacterial concentration (MBC)

Distinct antimicrobial susceptibility patterns were observed among the tested bacterial strains when exposed to iron oxide nanoparticles. Complete growth inhibition was found to be 1.9 µg/mL for all four bacterial strains. This is due to the 2-fold dilution system used in MIC assays. Consequently, the subtle difference near the inhibitory threshold might not be captured. This reflects the limitations of discrete dilution steps in the MIC method. Therefore, it does not imply identical susceptibility. With an IC50 value of 50.16 µg/mL,

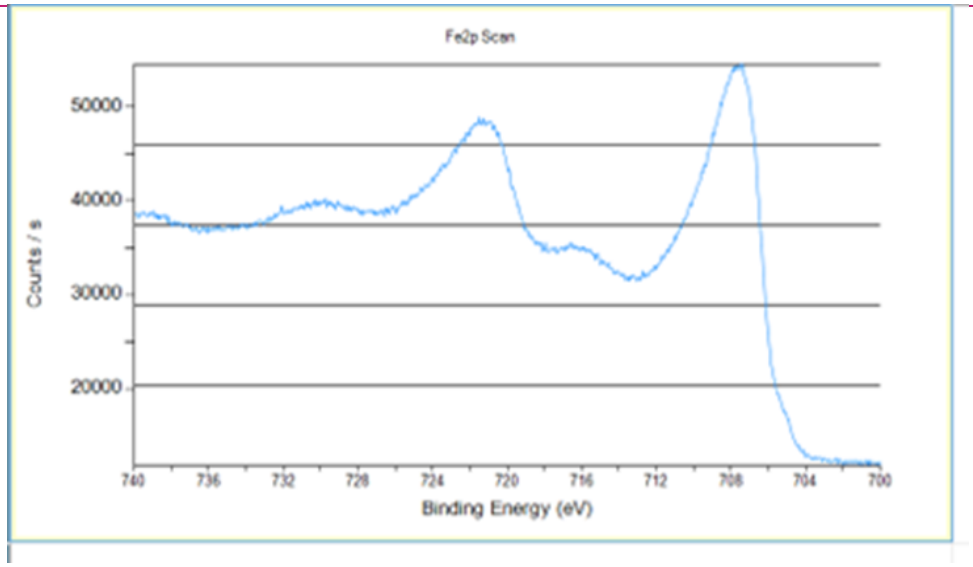

Fig. 7. *X-ray photoelectron spectroscopy (XPS) of iron element*

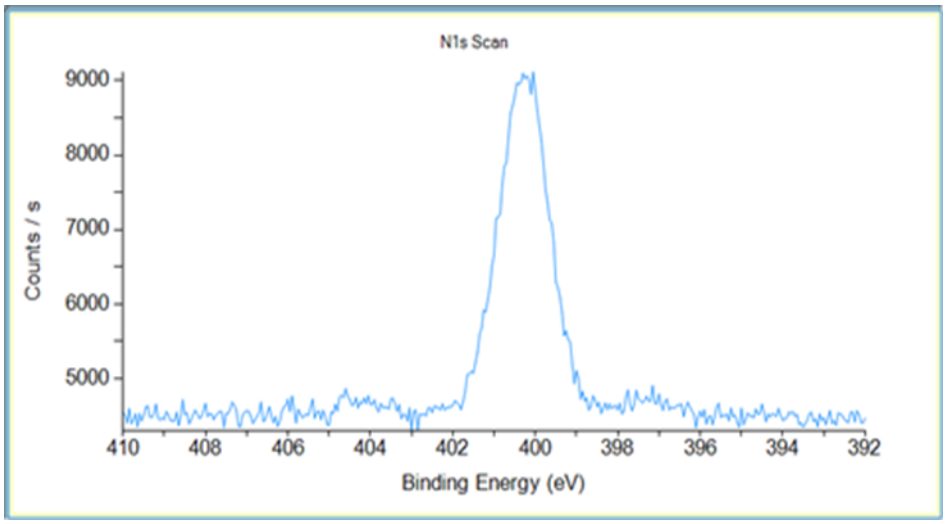

Fig. 8. *X-ray photoelectron spectroscopy (XPS) of nitrogen element*

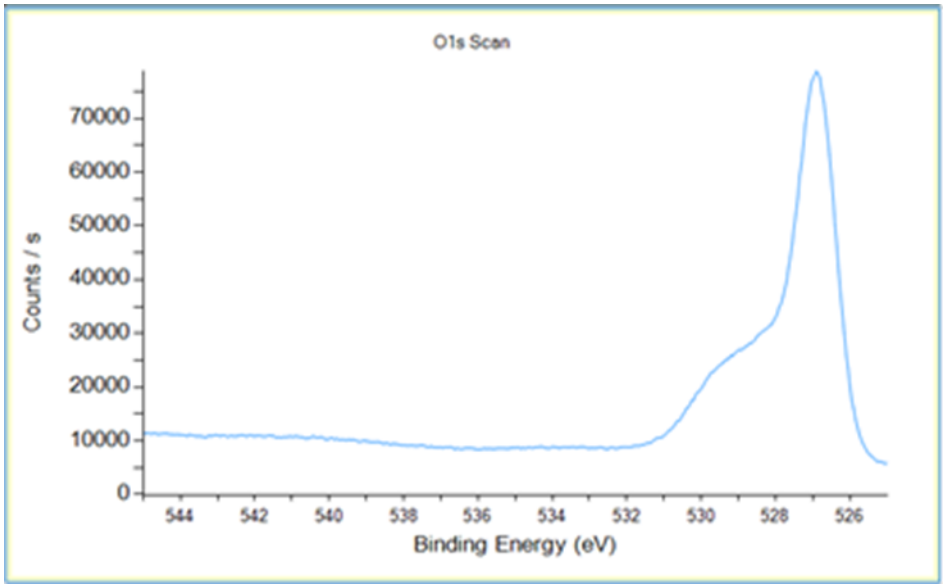

Fig. 9. *X-ray photoelectron spectroscopy (XPS)* of *oxygen element*

Table 1. Means ± SD of zone of inhibition obtained by iron oxide sample against Test organisms

S. No	Name of the test organism	Name of the test sample	Zone of inhibition (mm) Mean ± SD				
			1000µg/ml	500 µg/ml	250 µg/ml	100 µg/ml	PC
1.	*Streptococcus. aureus*	FeO	14.35±0.21	12.1±0.14	0	0	17.35±0.21
2.	*Streptococcus mutans*		14.45±0.35	12.6±0.14	7.6±0.14	0	16.75±0.35
3.	*Escherichia coli*		13.85±0.21	11.25±0.35	8.1±0.14	0	17.25±0.35
4.	*Pseudomonas aeruginosa*		13.6±0.14	10.85±0.49	0	0	16.1±0.14

Table 2. Minimum inhibitory concentration (MIC) and IC50 of iron oxide nanoparticles against multidrug-resistant bacteria

Bacterial Strain	Type	MIC (µg/mL)	IC50 (µg/mL)	Inhibition at 1.9 µg/mL (%)	Inhibition at 1000 µg/mL (%)
Streptococcus mutans	Gram positive	1.9	59.57	34.1	63.6
Staphylococcus aureus	Gram positive	1.9	50.16	5.2	75.3
Escherichia coli	Gram negative	1.9	135.5	19.0	74.8
Pseudomonas aeruginosa	Gram negative	1.9	156.1	30.3	86.5

Table 3. Percentage of antibiofilm efficacy of iron oxide nanoparticles against multidrug-resistant bacteria

Bacterial Strain	Type	Control OD (600nm)	IC50 (µg/ml)	Inhibition at 1000 µg/ml
Streptococcus mutans	Gram positive	2.246	25.41	71.35 %
Staphylococcus aureus	Gram positive	1.383	19.64	89.41 %
Escherichia coli	Gram negative	2.070	72.71	81.87 %
Pseudomonas aeruginosa	Gram negative	2.148	76.23	82.06 %

Staphylococcus aureus showed the maximum sensitivity, followed by *Streptococcus mutans* (IC50: 59.57 µg/mL), suggesting main antibacterial activity against Gram-positive organisms. The IC50 values for *Pseudomonas aeruginosa* and *Escherichia coli* were 156.1 µg/mL and 135.3 µg/mL, respectively (Table 2). Gram-negative organisms needed greater quantities of nanoparticles to effectively be killed.

This suggests that iron oxide is highly effective against those pathogenic organisms at very low concentrations. In his study, Wahran *et al.* (2024) reported "MIC values of 12.5, and 25 µg/ml for *E. coli*, and *P. aeruginosa*, respectively. Moreover, they added that, when combined with antibiotics, iron oxide nanoparticles significantly enhance the effectiveness of multiple antibiotics against multidrug-resistant bacteria. They suggested that iron oxide nanoparticles have promising applications as antibacterial compounds and as additives to enhance antibiotic efficacy". Al-Rawi *et al.* (2021) also reported that "the lowest MIC for synthesized Fe_3O_4NP (550µg/ml) was determined against *Pseudomonas aeruginosa* with 52±3.0 x10^3CFU, compared with untreated control (35±4.58 x10^6CFU)".

The total minimum bacterial concentration in the samples (S. mutans-FeO and S. aureus-FeO) was 1x10^2 CFU/mL. The total minimum bacterial concentration was present in the sample (E. coli-FeO and P. aeruginosa-FeO) was found to be 3x10^2 CFU/mL.

Antibiofilm

Different inhibitory profiles were found when the antibiofilm efficacy of IONPs was compared to four harmful bacterial strains: *E. coli-443*, P. *aeruginosa-424*, *S. aureus-902*, and *S. mutans-497* (Table 3). All studied strains showed concentration-dependent, varying-potency biofilm reduction by iron oxide. Iron oxide had minimal effect on *S. mutans* biofilm development at lower concentrations (1.9-3.9 µg/mL), however even at these concentrations, *S. aureus* was significantly inhibited. All strains showed increasingly stronger biofilm

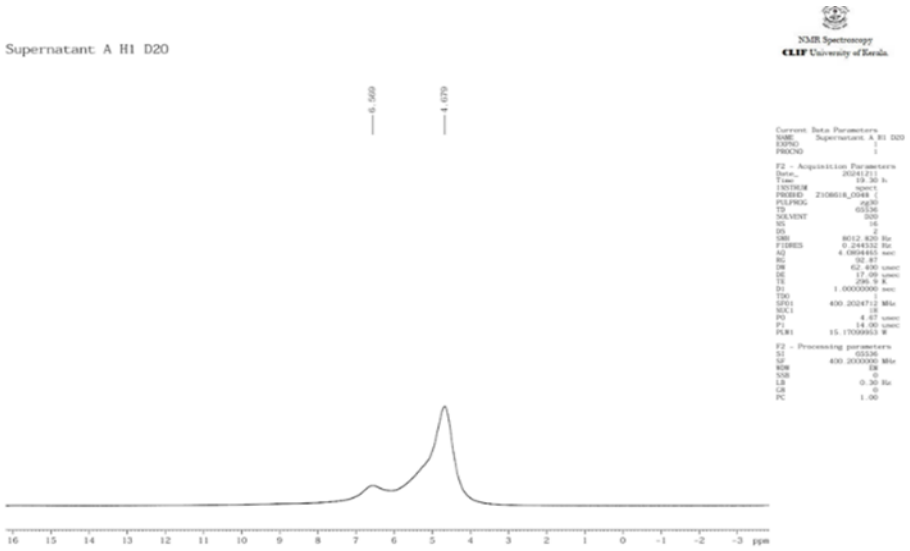

Fig. 10. *Nuclear magnetic resonance (NMR) spectrum of iron oxide nanoparticles*

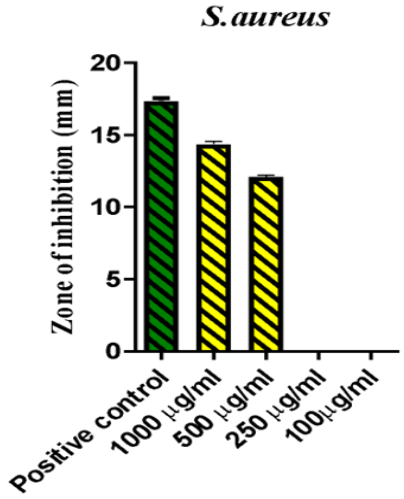

Fig. 11. *Antibacterial efficacy of iron oxide nanoparticles against Staphylococcus aureus*

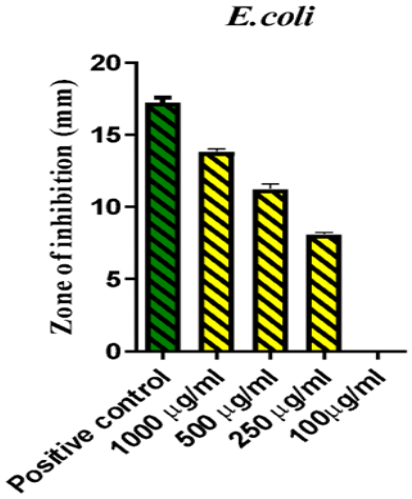

Fig. 12. *Antibacterial efficacy of iron oxide nanoparticles against Escherichia coli*

suppression as concentrations got higher, but *S. aureus* showed the highest sensitivity, with almost complete inhibition at the highest tested level (1000 µg/mL). Iron oxide nanoparticles worked especially well against Gram-positive bacteria, *S. aureus*. Variable reactions indicate that the structure of the bacterial cell wall and the composition of the biofilm may affect the mechanism of action of IONPs.

Harem *et al.,* (2024) noted that "α-FeO_3-NPs showed strong anti-biofilm activity against *E.coli* and *S. aureus"*. Sathyanarayanan *et al.* (2013) affirmed "the prevention of bacterial biofilm formation is strongly influenced by IONP. In addition to dispersion concentration, a prior study demonstrated that IONPs with diameters less than 10 nm significantly reduced bacterial biofilm growth. *P. aeruginosa* biofilm growth can be affected by IONPs at 10 µg mL-1, however biofilm formation was only significantly reduced at concentrations greater than 50 µg mL-1". Therefore, study conducted by Barcelos *et al.* (2025) , revealed that "IONPs with a diameter of 11.80 ± 3 nm and a concentration of 0.258 µg mL -1 prevented the formation of biofilms of *Pseudomonas aeruginosa"*.

Time killer assay

By monitoring OD600 (Fig. 15 a,b,c and d) (Table 4) and determining the percentage inhibition over a 24-hour period, the time-kill experiments assessed the antimicrobial activity of iron oxide nanoparticles against *S. mutans, S. aureus, E. coli*, and *P. aeruginosa* (Table 5). Over 24 hours, all strains (positive control) showed typical logarithmic growth, demonstrating a steady increase in OD, signifying typical bacterial growth. At each point, the iron oxide-treated sample showed noticeably lower OD values compared to the positive control, indicating that bacterial growth was inhibited. At all

Table 4. Inhibition of iron oxide nanoparticles against (a) *Psuedomonas aeruginosa*, (b) *Escherichia coli*, (c) *Staphylococcus aureus* and (d) *Staphylococcus mutans* (Time Killer Assay)

a

S.No	Time in Hours	OD value at 600 nm Control (in triplicates)			Mean value Control	OD value at 600 nm Sample (in triplicates)			Mean value Sample
1.	1	0.35	0.34	0.33	0.34 ± 0.01	0.20	0.19	0.27	0.22 ± 0.04
2.	6	0.72	0.79	0.83	0.78 ± 0.06	0.35	0.31	0.45	0.37 ± 0.07
3.	12	1.17	1.21	1.15	1.18 ± 0.03	0.41	0.49	0.55	0.48 ± 0.07
4.	24	1.32	1.33	1.39	1.35 ± 0.04	0.59	0.65	0.72	0.65 ±0.07

b

S.No	Time in Hours	OD value at 600 nm Control (in triplicates)			Mean value Control	OD value at 600 nm Sample (in triplicates)			Mean value Sample
1.	1	0.35	0.31	0.39	0.35 ± 0.04	0.23	0.29	0.22	0.25 ± 0.04
2.	6	0.76	0.81	0.77	0.78± 0.03	0.32	0.37	0.42	0.37 ± 0.05
3.	12	1.11	1.14	1.19	1.15 ± 0.04	0.44	0.45	0.52	0.47 ± 0.04
4.	24	1.34	1.29	1.38	1.34 ± 0.05	0.56	0.63	0.69	0.63 ± 0.07

c

S.No	Time in Hours	OD value at 600 nm Control (in triplicates)			Mean value Control	OD value at 600 nm Sample (in triplicates)			Mean value Sample
1.	1	0.34	0.32	0.29	0.32 ± 0.02	0.14	0.19	0.09	0.14 ± 0.05
2.	6	0.78	0.74	0.87	0.80 ± 0.07	0.22	0.27	0.32	0.27 ± 0.05
3.	12	0.97	1.07	1.10	1.05 ± 0.07	0.36	0.39	0.36	0.37 ± 0.02
4.	24	1.29	1.23	1.31	1.28 ± 0.04	0.49	0.43	0.52	0.48 ± 0.05

d

S.No	Time in Hours (h)	OD value at 600 nm Control (in triplicates)			Mean value Control	OD value at 600 nm Sample (in triplicates)			Mean value Sample
1.	1 h	0.36	0.39	0.29	0.35 ± 0.05	0.21	0.25	0.19	0.22 ± 0.03
2.	6 h	0.69	0.73	0.81	0.74 ± 0.06	0.27	0.31	0.38	0.32 ± 0.06
3.	12 h	1.06	1.17	1.08	1.10 ±0.06	0.43	0.48	0.53	0.48 ± 0.05
4.	24 h	1.33	1.26	1.22	1.27 ± 0.06	0.55	0.61	0.59	0.58 ± 0.03

time points, S. aureus showed the strongest inhibition (OD600 ~50–70% lower than the control). Moderate reduction of *S. mutans* and *P. aeruginosa* (~35–60% OD decrease). The weakest response was shown by *E. Coli*, which showed delayed inhibition (28% at 1 hour and 59% at 12 hours) (Table 4)

Kanish *et al.* (2024) observed in their study, "a noticeable reduction in *S.aureus* at all concentrations of Fe_2O_3 (25µg/ml, 50µg/ml and 100µg/ml) compared to the control. Iron oxide nanoparticles exhibit a dose-dependent antibacterial activity against *S. aureus*. At 100 µg/mL, *S.aureus* achieved a comparable reduction in CFU/mL. He concluded that iron oxide nanoparticles could be a potential alternative to traditional antibacterial agents in the treatment of infections caused by *S. aureus"*. On the other hand, they also observed "the reduction of *S.mutans*, reporting that the 50 µg/mL Fe2O3 NP treatment group shows a more noticeable decrease in CFU/mL count compared to the 25 µg/mL group, suggesting increased efficacy with a higher concentration. The 100 µg/mL iron oxide nanoparticles treatment shows the most significant decrease in CFU/mL count, indicating the highest level of antimicrobial activity among the tested nanoparticle concentrations".

DNA fragmentation

Based on the antibacterial activity of IONPs, *S. aureus* and *P. aeruginosa* that showed enhanced responses were selected for the DNA fragmentation assay. No DNA degradation was observed in the controls for S.

Table 5. Percentage of inhibition over 24 hours of iron oxide nanoparticles against multidrug-resistant bacteria

Bacterial Strain	1h	6h	12h	24h	Peak inhibition
Streptococcus mutans	37.3%	57.2%	56.4%	54.0%	57.2% (6h)
Staphylococcus aureus	56.1%	66.2%	64.6%	62.5%	66.2% (6h)
Escherichia coli	28.1%	52.6%	59.1%	53.1%	59.1% (12h)
Pseudomonas aeruginosa	35.1%	52.6%	58.9%	51.5%	58.9% (12h)

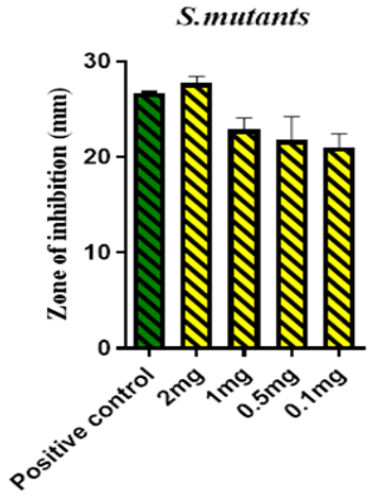

Fig. 13. *Antibacterial efficacy of iron oxide nanoparticles against Streptococcus mutans*

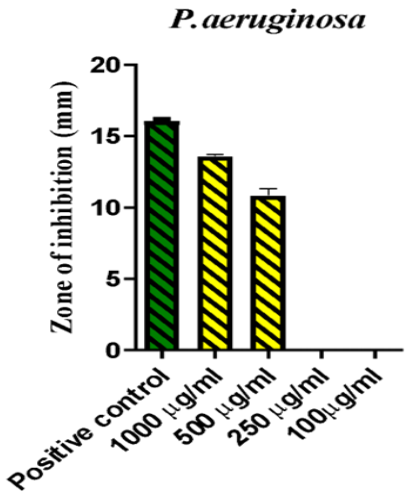

Fig. 14. *Antibacterial efficacy of iron oxide nanoparticles against Pseudomonas aeruginosa*

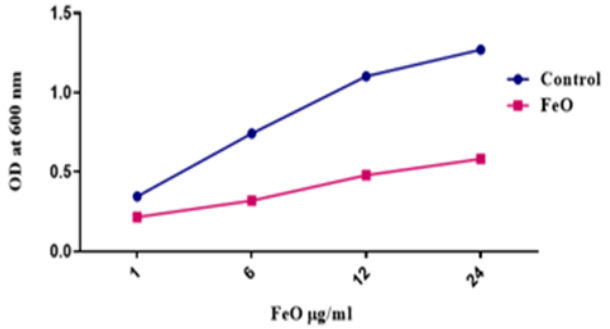

a. S. aureus

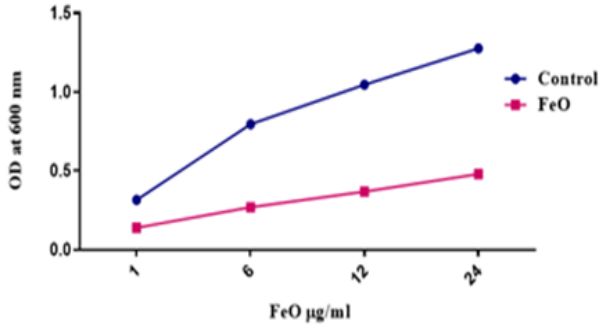

b. Streptococcus mutans

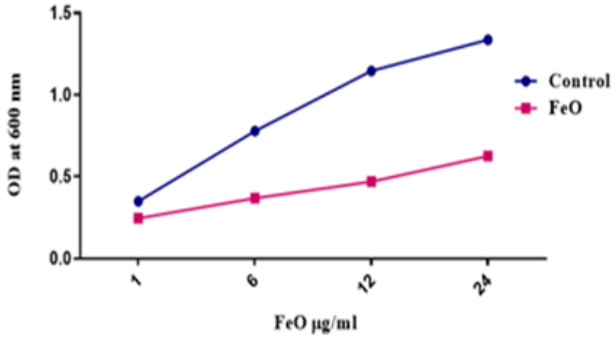

c. Escherichia coli

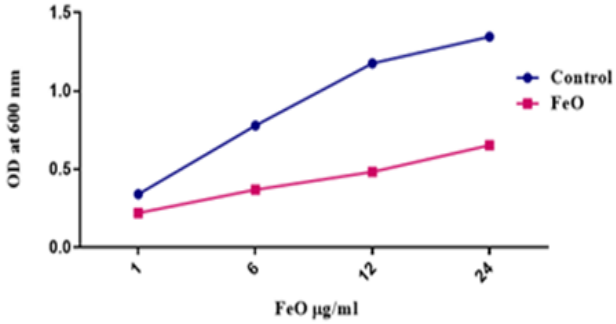

d. Pseudomonas aeruginosa

Fig. 15. *a, b, c, d: OD values (Control and FeO sample) depending on the concentration of iron oxide nanoparticles (Time Killer Assay)*

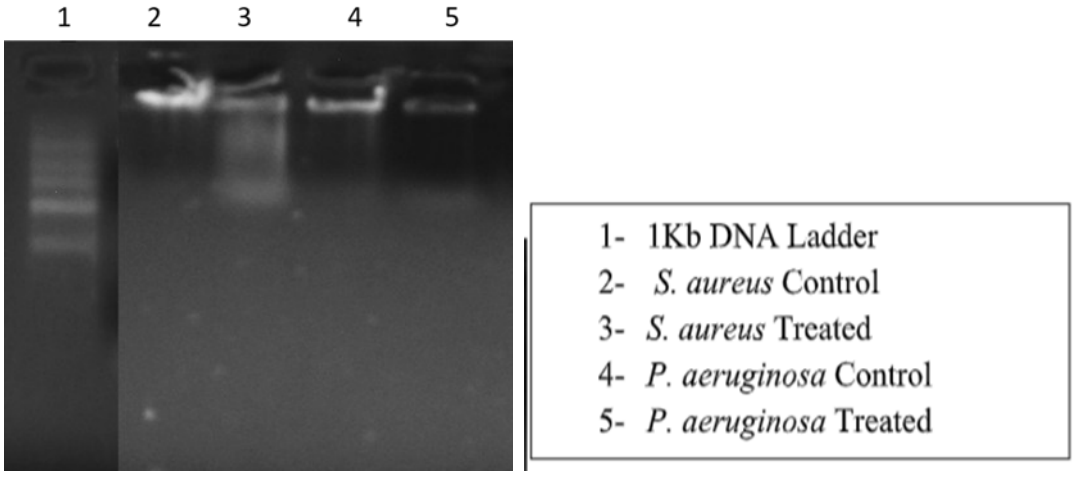

Fig. 16. *DNA fragmentation by gel electrophoresis of Staphylococcus aureus and Pseudomonas aeruginosa*

aureus and P. aeruginosa, which showed intact, high-molecular-weight genomic DNA as a single, clear band on agarose gel electrophoresis (Fig. 16). Following the treatment with the test substance the DNA fragmentation assay revealed distinct patterns of DNA fragmentation in both bacterial strains. For P. aeruginosa (lane 5), a faint but noticeable ladder-like pattern was observed indicating partial DNA cleavage or strain-specific sensitivity to nuclease activation. Treated S. aureus (lane 3) notably exhibited clear and intense DNA laddering, suggesting strong inhibition of programmed cell death (Fig. 16). These observations demonstrate that the test compound induces significant genomic DNA degradation, indicating a strong bactericidal effect on both organisms. Ghassan *et al.,* (2017), reported the results that "the iron oxide nanoparticles interacted with the DNA and changed its structure or conformation, which may have changed how the cell functions metabolically and damaged other parts of the cell". Sadeghi *et al.,* (2015) made a similar observation, reporting that "MNPs can start the DNA degradation process.

Conclusion

This study of chemically synthesised iron oxide nanoparticles (IONPs) showed that they have significant potential as a noble and antibacterial agent against multidrug-resistant pathogens. Characterization methods such as SEM, TEM, UV-Vis, FTIR, NMR, XRD, and XPS were used to confirm that the nanoparticles, which ranged in size to ±10 nm, exhibited a spherical or quasi -spherical shape and high crystallinity. Microbiological tests revealed concentration-dependent bactericidal effects and significant biofilm inhibition. Antibacterial efficacy against both Gram-positive (*S. mutans*, *S. aureus*) and Gram-negative (*E. coli*, *P. aeruginosa*) microorganisms were observed. Antibacterial activity was further validated by a DNA fragmentation assay, highlighting the nanoparticles' capacity to damage bacterial cells. The observed differences indicate that additional optimization is necessary to broaden efficacy, even though the microorganisms showed better sensitivity to IONPs. In the development of iron oxide-based antimicrobial agents to combat resistant bacterial infections, the present research results indicate that the proposed IONPs can be exciting alternatives to traditional antibiotics, offering multiple mechanisms, particularly with regard to genomic DNA damage. This work contributes to the field of nanobiotechnology by providing a strong foundation for the development of antimicrobial compounds based on IONPs to combat resistant bacterial infections.

ACKNOWLEDGEMENTS

We would like to evident our thankfulness to the assistants of the Department of Plant Production Technologies¸ Al- Furat Al- Awsat Technical University, Al-Mussaib Technical College, for their incorporeal and scientific corroboration.

Conflict of interest

The authors declare that they have no conflict of interest.

REFERENCES

1. Aarti Nughwal, Ruchi Bharti, Ajay Thakur, Monika Verma, Renu Sharma & Annu Pandey. (2025). Green synthesis of iron oxide nanoparticles from Mexican prickly poppy (Argemone mexicana): assessing antioxidant activity for potential therapeutic use. *RSC Adv.*, 15, 10287. DOI: 10.1039/d4ra07232d
2. Abdulrahman K. Ibrahim & Rasha Al Sahlanee. (2024). Wound healing and the antimicrobial impact by using biosynthesized iron oxide nanoparticles. *Iraqi Journal of Chemical and Petroleum Engineering*, 25,.4 147–155.

https://doi.org/10.31699/IJCPE.2024.4.14.

3. Adel A. M. Saeed, Eishah Mohammed Ali Mohsen & Abdul-Rahman Alawi Bin Yahia. (2025). Eco-friendly synthesis, characterization, and anticancer potential of iron oxide nanoparticles derived from Plectranthus amboinicus and Dorstenia foetida plant extracts, *Green Chemistry Letters and Reviews*, 18:1, 2525090, DOI: 10.1080/17518253.2025.2525090
4. Alok Mahato, Sudipa Manna, Sanjukta A. Kumar & Ashis Kumar Satpati. (2025). Probing the interaction of iron oxide nanoparticles (IONPs) with dsDNA in presence of UV–Vis light. *Surface Science and Technology*, 3:36 https://doi.org/10.1007/s44251-025-00102-8
5. Al-Rawi, Al-Mudallal N. H. A. L. & Taha A. A. (2021). Determination of ferrous oxide nanoparticles minimum inhibitory concentration against local virulent bacterial isolates. *Archives of Razi Institute*, 76, . 4 795-808. DOI: 10.22092/ari.2021.355997.1758.
6. Barcelos, A. F., Amaral, A. das G., Carneiro, L. C., Naves, P. L. F. & Guilherme, L. (2025). Synthesis and antimicrobial activity of iron oxide/silver nanocomposites against *Pseudomonas aeruginosa* biofilms. *Ciencia e Natura*, 47, e84264. DOI: https://doi.org/10.5902/2179460X84264. Available in: https://doi.org/10.5902/2179460X84264
7. Bashiru Ibrahim, Taiwo Hassan Akere & Hanene Ali-Boucette. (2023). Gold nanoparticles induced size dependent cytotoxicity on human alveolar adenocarcinoma cells by inhibiting the ubiquitin proteasome system, *Pharmaceutics*, 15, 432.http://doi.org/10.3390/pharmaceutics15020432.
8. Bauer, A. W., C. E. Roberts Jr & W. M. Kirby. (1959). Single disc versus multiple disc and plate dilution techniques for antibiotic sensitivity testing. *Antibiotics Annual* , 7 : 574-580.
9. Bristy Biswas, Md. Lutfor Rahman, Md. Farid Ahmed & Nahid Sharmin. (2024). Extraction of gamma iron oxide (γ-Fe2O3) nanoparticles from waste can: Structure, morphology and magnetic properties. *Heliyon,* 10. https://doi.org/10.1016/j.heliyon.2024.e30810.
10. Darezereshki E. (2011). One-step synthesis of hematite (a-Fe2O3) nano-particles by direct thermal-decomposition of maghemite. *Mater Lett*., 65:642–5. https://doi.org/10.1016/j.matlet.2010.11.030.
11. Gang Wang, Guobin Song & Yuanhong Xu. (2021). A rapid antimicrobial susceptibility test for *Klebsiella pneumoniae* using a broth micro-dilution combined with MALDI TOF MS. *Infect Drug Resist*, 14: 1823–1831.
12. Ghassan M. Sulaiman, Amer T. Tawfeeq & Amal S. Naji. (2017). Biosynthesis, characterization of magnetic iron oxide nanoparticles and evaluations of the cytotoxicity and DNA damage of human breast carcinoma cell lines. *Artificial Cells, Nanomedicine, and Biotechnology*, 46:6, 1215-1229. DOI: 10.1080/21691401.2017.1366335.
13. Gregory P. Lopinski, Oltion Kodra, Filip Kunc, David C. Kennedy, Martin Couillard & Linda J. Johnston. (2025). X-ray photoelectron spectroscopy of metal oxide nanoparticles: chemical composition, oxidation state and functional group content. *Nanoscale Adv*., 7, 1671. DOI: 10.1039/d4na00943f
14. Gupta P., K. Mishra, A. K. Mittal, N. Handa & M. K. Paul. (2024). Current expansion of silver and gold nanomaterials towards cancer theranostics: Development of therapeutics. *Curr. Nanosci.*, 20, 356.
15. Harem Jamal Fatih, Morahem Ashengroph, Aram Sharifi & Musa Moetasam Zorab. (2024). Green-synthesized α-Fe2O3-nanoparticles as potent antibacterial, anti-biofilm and antivirulence agents against pathogenic bacteria. *BMC Microbiology*, 24:535. https://doi.org/10.1186/s12866-024-03699-2.
16. M. Heggen, J.E. Martinez Medina, A.M. Philippe & E. Barborini. (2025). Experimental insights on the stability of core–shell structure in single Sn/ SnOx spherical nanoparticles during room temperature oxidation. *Applied Surface Science, Elsevier*, 684, 161984
17. Hend Algadi, Mohammed Abdelfatah Alhoot, Anis Rageh Al-Maleki & Neny Purwitasari. (2024). Effects of metal and metal oxide nanoparticles against biofilm-forming bacteria: A systematic review. *J. Microbiol Biotechnol.,* 15;34(9):1748-1756. https://doi.org/10.4014/jmb.2403.03029.
18. Johar Amin Ahmed Abdullah, Cesar Andre Andino Perdomo, Luis Arturo Hernandez Núnez, Octavio Rivera-Flores, Marlon Sanchez-Barahona, Antonio Guerrero & Alberto Romero. (2024). Lychee peel extract-based magnetic iron oxide nanoparticles: Sustainable synthesis, multifaceted antioxidant system, and prowess in eco-friendly food preservation. *Food and Bioproducts Processing*, 145 148–157. https://doi.org/10.1016/j.fbp.2024.03.007.
19. Justin C., Sheryl Ann Philip & Antony V. Samrot. (2017). Synthesis and characterization of superparamagnetic iron-oxide nanoparticles (SPIONs) and utilization of SPIONs in X-ray imaging, *Appl Nanosci*, 7 :463-475. DOI 10.1007/s13204-017-0583-x.
20. Kamath V., P. Chandra, & G.P. Jeppu. (2021). Comparative study of using five different leaf extracts in the green synthesis of iron oxide nanoparticles for removal of arsenic from water, *Int. J. Phytoremediation*, 22 1278–1294. https://doi.org/10.1080/15226514.2020.1765139.
21. Kanish.S, Subramanian R.M., Rajeshkumar Shanmugam & Sulochana Govindharaj. (2024). In vitro antibacterial activity of iron oxide nanoparticles synthesised using hydrocotyle umbellata L. against oral pathogens. *Nanotechnology Perceptions*, ISSN 1660-6795.
22. Laurence M. Harwood & Timothy D. W. Claridge. (1996). Introduction to organic spectroscopy. Oxford University Press.
23. Maria Jose Inestrosa-Izurieta, Diego Vilches & Julio I, Urzua. (2023). Tailored synthesis of iron oxide nanoparticles for specific applications using a statistical experimental design, *Heliyon*, 9, 11. https://doi.org/10.1016/j.heliyon.2023.e21124
24. Muhammad Israeel, Javed Iqbal, Banzeer Ahsan Abbasi, Shumaila Ijaz, Rafi Ullah, Farishta Zarshan, Tabassum Yaseen, Gul Khan, Ghulam Murtaza, Iftikhar Ali, Khalou Mohammed Alarjani, Mohamed S Elshikh, Muhammad Rizwan, Shoaib Khan & Rashid Iqbal. (2024). Potential biological applications of environment friendly synthesized iron oxide nanoparticles using *Sageretia thea* root extract. *Scientific Reports*, 14, Article number: 28310. https://doi.org/10.1038/s41598-024-79953-4
25. Priyanka Singh, Santosh Pandit, Sri Renukadevi Balusamy, Mukil Madhusudanan, Hina Singh, H. Mo-

hamed Amsath Haseef & Ivan Mijakovic. (2024). Advanced nanomaterial for cancer therapy: Gold, Silver and Iron oxide nanoparticles in oncology application. *Advanced Healthcare Materials*, 14, 4. DOI: 10.1002/adhm.202403059

26. Rajeshkumar Shanmugam, M. Tharani, Shahabe Saquib Abullais, Santosh R. Patil, & Mohmed Isaqali Karobari. (2024). Black seed assisted synthesis, characterization, free radical scavenging, antimicrobial and anti-inflammatory activity of iron oxide nanoparticles. *BMC Complementary Medicine and Therapies.* 24:241. https://doi.org/10.1186/s12906-024-04552-9
27. Rimbu M.C., Cord D., Savin M., Grigoroiu A., Mihaila M.A., Galatanu M.L., Ordeanu V., Panturoiu M., T, Ucureanu V. & Mihalache I. (2025). Harnessing plant-based nanoparticles for targeted therapy: A green approach to cancer and bacterial infections. *Int. J. Mol. Sci.* 26, 7022. https:// doi.org/10.3390/ijms26147022
28. Sahar Q. Abas, Mais E. Ahmed & Mazin K. Hamid. (2025). Ultrasound-assisted synthesis of iron oxide nanoparticles: Application in cytotoxicity and antibacterial activity. *Iraqi JMS*,. 23(1)
29. Sambrook, J. & Russell, D.W. (2021). Molecular cloning: A laboratory manual. 3rd Edition, 1 Cold Spring Harbor Laboratory Press, New York
30. Sathyadevi Palanisamy & Yun-Ming Wang. (2019). Superparamagnetic iron oxide nanoparticulate system: synthesis, targeting, drug delivery and therapy in cancer, *Dalton Trans.* 48, 9490
31. Sathyanarayanan M. B., Balachandranath R., Genji Srinivasulu Y., Kannaiyan S. K., & Subbiahdoss G. (2013). Effect of gold and iron-oxide nanoparticles on biofilm-forming pathogens. *International Scholarly Research Notices*. http://dx.doi.org/10.1155/2013/272086.
32. Silvia Groiss, Raja Selvaraj, Thivaharan Varadavenkatesan & Ramesh Vinayagam. (2017). Structural characterization, antibacterial and catalytic effect of iron oxide nanoparticles synthesized using the leaf extract of *Cynometra ramiflora. Journal of Molecular Structure.* 1128, 572-578. https://doi.org/10.1016/j.molstruc.2016.09.031
33. Tsuji, Brian T., Jenny C. Yang, Alan Forrest, Pamela A. Kelchlin & Patrick F. Smith. (2008). "In vitro pharmacodynamics of novel rifamycin ABI-0043 against *Staphylococcus aureu*s." *Journal of Antimicrobial Chemotherapy*, 62, no. 1: 156-160. https://doi.org/10.1093/jac/dkn133
34. Wahran M. Saod, Mohammed Salih Al-Janaby, Estabraq W. Gayadh, Asmiet Ramizy & Layth L. (2024). Biogenic synthesis of iron oxide nanoparticles using *Hibiscus sabdariffa* extract: Potential for antibiotic development and antibacterial activity against multidrug-resistant bacteria. *Current Research in Green and Sustainable Chemistry,* 8 100397. https://doi.org/10.1016/j.crgsc.2024.100397
35. Wang, Qian, Feng-Jun Sun, Yao Liu, Li-Rong Xiong, Lin-Li Xie & Pei-Yuan Xia. (2010). Enhancement of biofilm formation by subinhibitory concentrations of macrolides in icaADBC-positive and-negative clinical isolates of *Staphylococcus* epidermidis. *Antimicrobial Agents and chemotherapy*. 54, no. 6: 2707-2711. https://doi.org/10.1128/aac.01565-09.